Communication

Broadband High-Gain SIW Horn Antenna Loaded With Tapered Multistrip Transition and Dielectric Slab for mm-Wave Application

Yaling Chen, Long Zhang, Yejun He, Chunxu Mao, Sai-Wai Wong, Wenting Li, Peng Chu, and Steven Gao

***Abstract*— A substrate integrated waveguide (SIW) H-plane horn antenna loaded with tapered multistrip transition and dielectric slab is proposed for broadband high-gain operation. The broadband characteristic of the proposed antenna is obtained by loading a tapered multistrip transition. The theory of coupled resonator is introduced to reveal the mechanism of bandwidth enhancement. On the other hand, a dielectric slab is used to enhance the gain of the proposed antenna. The optimal length of this dielectric slab is determined based on the design principles of a dielectric rod with maximum gain. Besides, the tapered multistrip transition also contributes to the gain improvement by suppressing the feed radiation and prompting the transverse expansion of the surface wave. To verify the design theory and concept, a prototype operating at the K- and Ka-bands is fabricated and measured. The measurement results show that the impedance bandwidth of the proposed antenna is from 20.6 to 38.4 GHz (60%). Within the operating band, a peak realized gain of 19.1 dBi and excellent endfire radiation patterns with low cross polarization (<−30 dB) and high front-to-back ratio (FBR > 20 dB) are achieved simultaneously. With its broad bandwidth, high gain, low cross polarization, and high FBR, the proposed antenna is promising for various millimeter-wave applications.**

***Index Terms*— Dielectric slab loading, horn antenna, millimeter-wave (mm-wave) antenna, substrate integrated waveguide (SIW), tapered multistrip transition.**

I. Introduction

Horn antennas are extensively used in various systems, such as the radar and wireless communication systems. However, the conventional horn antennas are developed from bulky flared waveguide structures, which limit their applications in the planar integrated circuits. To integrate with planar circuits, substrate integrated waveguide (SIW)-based horn antennas were developed [1]. Unlike the bulky metallic horn antennas, the SIW horn antenna is planar, lightweight, and convenient to constitute antenna array. However, due to the mismatch between the substrate and the air at the horn aperture, the SIW horn antenna features narrow impedance bandwidth (IBW) and low gain [2]. To overcome these issues, a variety of efforts have been devoted, including use of various impedance transformers [2]–[4], ridged SIW [5], dielectric loading technique [6], various phase correction structures [7], [8], and so on.

To the best knowledge of the authors, the maximum reported bandwidth of nonridged SIW horn antenna remains less than 50% [4]. Some designs have achieved more than 75% IBW using the ridged SIW technology, but multilayer substrate or stepped substrate was essential to implement the ridged SIW, which was rather complex and costly [5]. Regarding the gain performance, the reported single-layer SIW horn antennas generally featured a peak gain of less than 15 dBi [6], [7]. In view of this, the aim of this work is to design a single-layer SIW horn antenna with both broad IBW (>50%) and high antenna gain (>15 dBi).

In this communication, a novel SIW H-plane horn antenna loaded with tapered multistrip transition and dielectric slab is proposed. The tapered multistrip transition is inspired by the traditional uniform printed transition [2], but has more transition blocks which facilitate the bandwidth improvement. The theory of coupled resonator is used to reveal the impedance matching mechanism of the proposed transition. Besides, a dielectric slab is used to further increase the antenna gain. Based on the design principle of a dielectric rod with maximum gain, the optimal length of this dielectric slab is determined. Then, the gain enhancement of the proposed antenna is investigated by the modal analysis of the tapered multistrip transition. With the coexistence of the tapered multistrip transition and the dielectric slab, wide IBW, high antenna gain, and symmetrical endfire radiation pattern with low cross polarization and high front-to-back ratio (FBR) are obtained simultaneously by the proposed design. Due to these advantageous features, the proposed SIW horn antenna can find applications in various millimeter-wave (mm-wave) systems, such as the 5G mobile communications and high data-rate Satcoms.

II. Antenna Design and Impedance Matching

A. Design of the SIW H-Plane Horn

The geometry of the proposed SIW H-plane horn is illustrated in Fig. 1. As shown, the antenna consists of five parts: the grounded coplanar waveguide (GCPW), the GCPW-SIW transition, the SIW H-plane horn, the tapered multistrip transition, and the extended dielectric slab. All the parts are constructed on a 1.524 mm-thick Rogers RO4003C substrate with a permittivity of 3.55 and a loss tangent of 0.0027. The proposed SIW H-plane horn is designed according to the theory presented in [9]. For high aperture efficiency and gain, the optimum length of the SIW H-plane horn is given as follows:

$$l_4 = \frac{w_0^2}{3\lambda_d} \tag{1}$$

where λ_d is the guided wavelength in the dielectric substrate, and w_0 is the width of the SIW horn aperture.

Manuscript received 16 April 2021; revised 19 February 2022; accepted 27 February 2022. Date of publication 28 March 2022; date of current version 26 July 2022. This work was supported in part by the National Natural Science Foundation of China under Grant 61801299 and Grant 62071306, in part by the Natural Science Foundation of Guangdong Province under Grant 2020A1515011037, and in part by the Shenzhen Science and Technology Program under Grant JCYJ20200109113601723 and Grant JSGG20210420091805014. *(Corresponding author: Long Zhang.)*

Yaling Chen, Long Zhang, Yejun He, Sai-Wai Wong, and Wenting Li are with the College of Electronics and Information Engineering, Shenzhen University, Shenzhen 518060, China (e-mail: long.zhang@szu.edu.cn; heyejun@126.com).

Chunxu Mao is with the 5G Innovation Centre (5GIC), Institute for Communication Systems (ICS), University of Surrey, Guildford GU2 7XH, U.K.

Peng Chu is with the College of Electronic and Optical Engineering, Nanjing University of Posts and Telecommunications, Nanjing 210023, China.

Steven Gao is with the School of Engineering and Digital Arts, University of Kent, Canterbury CT2 7NT, U.K. (e-mail: s.gao@kent.ac.uk).

Color versions of one or more figures in this communication are available at https://doi.org/10.1109/TAP.2022.3161349.

Digital Object Identifier 10.1109/TAP.2022.3161349

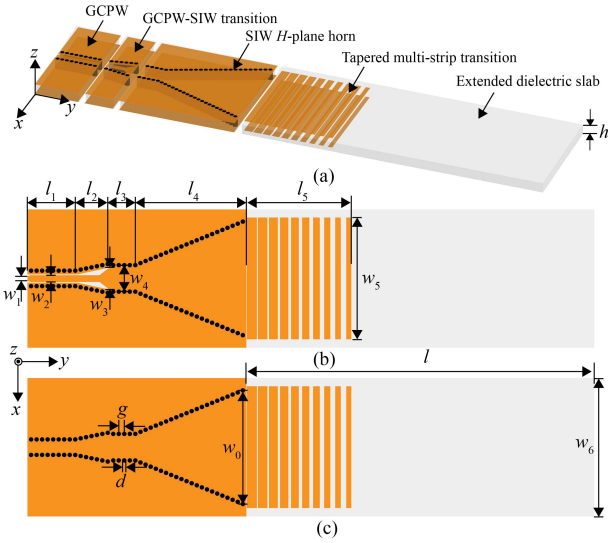

Fig. 1. Geometry of the proposed SIW horn antenna. (a) Exploded view. (b) Top view. (c) Bottom view. (Geometrical dimensions, all units are in mm: $l_1 = 8.65$, $l_2 = 5.88$, $l_3 = 5$, $l_4 = 20.1$, $l_5 = 19$, $l = 63$, $h = 1.524$, $w_0 = 20.53$, $w_1 = 0.8$, $w_2 = 1.2$, $w_3 = 4$, $w_4 = 4.8$, $w_5 = 22$, $w_6 = 25$, $g = 1$, and $d = 0.8$).

B. Design of the Tapered Multistrip Transition

To improve the impedance matching between the substrate and the air at the SIW horn aperture, printed transitions can be used. A traditional printed multistrip transition with a fixed slot width is shown in Fig. 2(a). The traditional printed transition was introduced previously in [2] and [3], where it was placed after the horn aperture to generate additional resonances. For example, the shifted resonant frequencies $f_{r2\pm}$ of a uniform two-block transition can be estimated by [2]

$$f_{r2\pm} = \frac{f_{r1}}{\sqrt{1 \mp k_2}} \tag{2}$$

where f_{r1} is the resonant frequency of single uncoupled block, and k_2 is the coupling factor between the two blocks. Using printed transition, the antenna IBW was successfully improved to around 16% [3]. However, the bandwidth was not further improved when the number of transition blocks exceeded three. Conversely, adding more blocks would result in poorer bandwidth performance [2].

To further enhance the impedance matching of printed transition with more than three blocks, a tapered multistrip transition is proposed, which greatly improves the IBW of SIW horn. The configuration of the proposed transition is shown in Fig. 2(b). As shown, there are n transition blocks placed on the extended dielectric slab at the horn aperture. Each block is constituted by a pair of parallel slots and a pair of parallel strips. The width of the i th slot is denoted by s_i $(i = 1, 2, \ldots, n)$, while the width of the strip is denoted by t_i. The width of each block is kept fixed as p, and its length is denoted by w_5.

C. Impedance Matching Mechanism

Since the printed transition is viewed as a coupled resonator, only the printed transition is taken into account to illustrate its resonant characteristics at first. The simulation models of the traditional uniform multistrip transition and the proposed tapered multistrip transition are presented in Fig. 3(a) and (b), respectively. The simulated reflection coefficients of the traditional uniform transition and the proposed tapered multistrip transition with different block numbers n are shown in Fig. 4. As shown, the impedance matching is improved

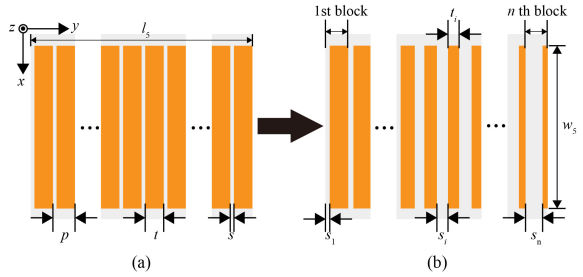

Fig. 2. Configuration of: (a) traditional printed multistrip transition and (b) tapered multistrip transition.

Fig. 3. Simulation models of (a) uniform multistrip transition and (b) tapered multistrip transition with n blocks.

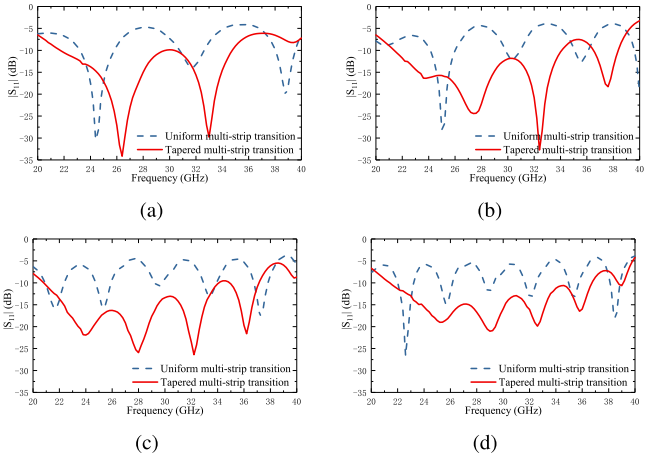

Fig. 4. Simulated $|S_{11}|$ of both the transitions with different block numbers (n). (a) $n = 4$. (b) $n = 6$. (c) $n = 8$. (d) $n = 10$ ($p = 1.9$ mm, $s = 0.1$ mm, $s_i = s + (i - 1) \times 0.1$ mm).

greatly with the increase in block numbers for the proposed tapered multistrip transition. On the contrary, even with the use of ten blocks, only six separated operating bands are obtained for the traditional uniform transition as illustrated in Fig. 4(d). The reason for this phenomenon can be explained as follows.

The resonant frequencies of printed transition are determined by the self-resonance frequency of the uncoupled block and the coupling factor $k_{(i,i+1)}$ between two adjacent blocks, which are mainly determined by the strip widths and slot widths [2]. In our work, the tapered multistrip transition with decreasing strip widths and increasing slot widths is used to simultaneously change the self-resonance frequency of each block and the coupling coefficient $k_{(i,i+1)}$. With the decrease in strip widths and the increase in slot widths, the value of $k_{(i,i+1)}$ reduces, which decreases the frequency gap of two adjacent resonances. As the frequency gap of two adjacent resonances decreases, these two resonances can be more easily merged to realize a wide bandwidth. Take the two transitions with four blocks as an example, the corresponding $|S_{11}|$ are shown in Fig. 4(a). As shown, the frequency gaps of two adjacent resonances of the proposed tapered transition are 6.6 and 6.2 GHz, respectively. However, the frequency gaps of the uniform transition are 7.43 and 7.08 GHz, respectively. As expected, the bandwidth of the tapered transition is much wider than that of the uniform one.

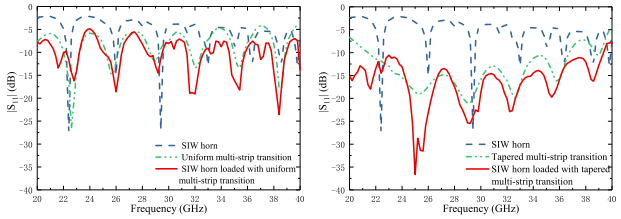

Fig. 5. Simulated $|S_{11}|$ of the SIW horn loaded with/without (a) uniform multistrip transition and (b) tapered multistrip transition (both the transitions have ten blocks).

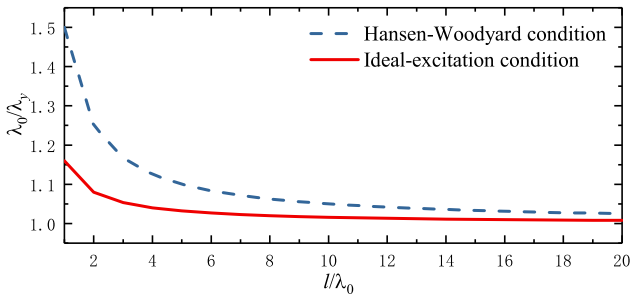

Fig. 6. λ_0/λ_y for maximum-gain surface wave antennas as a function of relative rod length l/λ_0.

To investigate the effect of the two transitions on the impedance matching of the proposed SIW horn, $|S_{11}|$ of the proposed SIW horn with and without transitions are shown in Fig. 5. As shown, the bandwidth of the SIW horn loaded with printed transition is determined by the resonant characteristics of both the SIW horn and the printed transition. In Fig. 5(a), by loading uniform transition, only seven separated narrow operating frequency bands are obtained. On the contrary, the IBW of the SIW horn is effectively broadened by the additional resonances of the tapered multistrip transition, as illustrated in Fig. 5(b). Therefore, it is evident that the proposed tapered multistrip transition can greatly enhance the poor matching of SIW horn. Moreover, the tapered multistrip transition also contributes to gain enhancement, which is discussed subsequently.

III. Gain Enhancement

A. Optimum Length of the Extended Dielectric Slab

As shown in Fig. 1(a), an extended dielectric slab is placed in front of the SIW horn aperture to improve the antenna radiation performance. The extended dielectric slab can be viewed as a dielectric rod. The reason for gain improvement using the dielectric slab is that a secondary Huygens plane exists in the terminal aperture of the dielectric slab [11]. For the extended dielectric slab, a part of the input power is converted into the surface wave, and the efficiency of surface wave conversion (the ratio of power in the surface wave to the total input power) is usually between 65% and 75% [12]. The rest of the power is directly radiated near the SIW horn aperture, which is called as the feed radiation. Therefore, the amplitude of the electric field along the dielectric slab starts with a hump near the SIW horn aperture and flattens out with the increasing length of the dielectric slab. In this case, the maximum gain would be obtained by meeting the Hansen–Woodyard condition. This requires the phase difference between the surface wave and the free-space wave from the feed to be approximately 180° at the end of antenna [12]

$$lk_y - lk_0 = \pi \tag{3}$$

or equivalently

$$\frac{\lambda_0}{\lambda_y} = 1 + \frac{\lambda_0}{2l} \tag{4}$$

where k_y and k_0 are the wave numbers along the y-direction and in the free space, respectively, and l is the total length from the horn aperture to the end of the antenna. Under the Hansen–Woodyard condition, there is no strict requirement for the efficiency of surface wave conversion. If the efficiency of surface wave conversion is rather high (approximately 100%), or the feed radiation is effectively suppressed, an ideal excitation condition with maximum gain could be obtained [12], that is,

$$\frac{\lambda_0}{\lambda_y} = 1 + \frac{\lambda_0}{6l} \tag{5}$$

Fig. 6 shows the relationship between λ_0/λ_y and l/λ_0. As shown, for any given length l, λ_0/λ_y values under the ideal excitation condition are smaller than that under the Hansen–Woodyard condition. In [13], experimental study shows that the terminal phase difference of a dielectric rod can be nearly 180° for $l = 20\lambda_0$, which satisfies the Hansen–Woodyard condition with maximum gain. It is noted that for the Hansen–Woodyard condition with $l = 20\lambda_0$, the value of λ_0/λ_y is 1.025, which is approximately equivalent to the ideal excitation condition with $l = 6\lambda_0$, where λ_0/λ_y is 1.026. According to the equivalence principle, the optimal length l for the ideal excitation condition can be selected as $6\lambda_0$ in this case. Apparently, for achieving a certain maximum gain, the required slab length under the ideal excitation condition is much shorter than that under the Hansen–Woodyard condition.

To meet the ideal excitation condition, a tapered dielectric rod was usually used to increase the efficiency of surface wave excitation [12]. However, this will yield complex antenna structure. In this work, a ten-block tapered multistrip transition is printed after the horn aperture to realize the ideal excitation condition without tapering the dielectric slab. It is found that a smooth transition from the waveguide mode to the surface wave mode is obtained by the proposed transition, which facilitates the realization of the ideal excitation condition. To verify this, the operational modes of the proposed transition are analyzed in Section III-B.

B. Modal Analysis of the Tapered Multistrip Transition

Considering that the E-field distribution along the tapered transition is symmetrical about the middle plane of the substrate, the middle plane thus serves as a perfect electric wall (PEC) [10], as shown in Fig. 7(a). In this case, only the upper half part of the fields needs to be taken into account according to the image theory. Consequently, the height of the proposed transition can be reduced to one half with the bottom plane replaced by a metallic ground plane. The simplified model of the proposed transition is shown in Fig. 7(b), which can be considered as a slotted parallel plate waveguide (PPW). The unit cell of the slotted PPW is shown in Fig. 7(c).

The dispersion characteristics of the unit cell are calculated by Mehdipour and Eleftheriades [14]

$$|\beta_{eff}| = \frac{1}{p}\,\mathrm{Re}\left[\cos^{-1}\left(\frac{A+D}{2}\right)\right] \tag{6}$$

where β_{eff} is the effective phase constant. A and D are the elements of the ABCD matrix of the unit cell, and p is the period of the unit cell. It is known that the slotted PPW can support a leaky-wave mode, a proper waveguide mode, and a surface wave mode [10]. When $|\beta_{eff}|/k_0 < 1$, electromagnetic (EM) waves from the slotted PPW propagate as fast waves (leaky-wave mode) which can be radiated from the slotted PPW. The proper waveguide mode occurs when

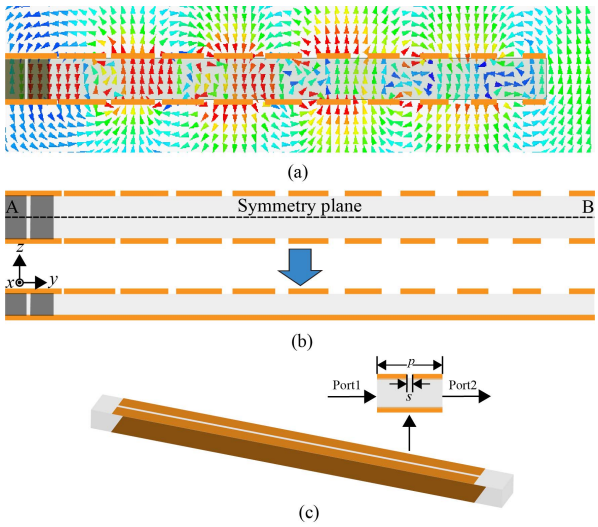

Fig. 7. (a) E-field distribution along the tapered transition at 29 GHz. (b) Simplified model of the tapered transition. (c) Unit cell.

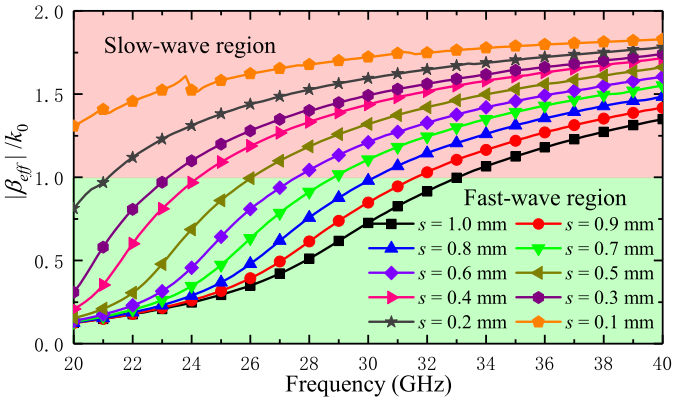

Fig. 8. Dispersion diagram of the unit cell with different slot widths.

$|\beta_{eff}|/k_0 > 1$ (slow wave), where most of the power is stored inside the slotted PPW. Besides, the surface wave mode also appears in the slow wave region, and most of surface wave power is stored at the surface of the slotted PPW.

Based on (6), the dispersion diagram of the unit cell with different slot widths (s) is shown in Fig. 8. Take the slot width $s = 0.8$ mm as an example, the unit cell supports two modes: a leaky-wave mode in the frequency range of 20–30 GHz and a proper mode (proper waveguide mode or surface wave mode) in the frequency range of 30–40 GHz. The leaky-wave mode can be radiated from the slotted PPW [14], while the proper mode guides the EM waves from the feed to the end of antenna. When $|\beta_{eff}|/k_0 > 1$, the leaky mode starts to lose its physical significance, but the proper mode begins to contribute to endfire radiation. Therefore, Fig. 8 indicates that the operating modes for different transition blocks are varied. For instance, at 30 GHz, the first eight blocks operate in the proper mode, while the last two blocks work in improper leaky mode. It is also shown in Fig. 8 that the number of blocks operating in the proper mode increases with the increase in frequency. Apparently, the proposed transition can support both the proper mode and the leaky-wave mode in the frequency range of 20–33 GHz, but only the proper mode in the frequency range of 33–40 GHz.

Since the proper mode can guide the EM waves from the feed to the dielectric slab, the existence of the proper mode facilitates power transmission along the dielectric slab. Besides, the experimental study has shown that the leaky-wave mode contributes to the expansion of fields [15]. The coexistence of the proper mode and improper leaky-wave mode in the proposed transition serves two purposes. First, with the existence of the proper mode, the majority of the power is guided from the SIW horn to the extended dielectric slab and the efficiency of surface wave excitation is increased, which helps meet the ideal excitation condition and yields a maximum endfire gain. Second, the leaky-wave mode is used to expand the equiphase region of the surface wave in the transverse direction, thereby increasing the size of the effective aperture at the extended dielectric slab and consequently improving the gain.

Fig. 9 shows the magnitude of electric fields in the E-plane of the dielectric-loaded SIW horn antenna with and without tapered transition. As shown in Fig. 9(a), when the SIW horn is not loaded with tapered transition, part of the power that cannot be converted into the surface wave is radiated near the SIW horn aperture. Consequently, the feed radiation is generated, which radiates toward the back side of the dielectric slab and interferes with the fields propagating in the forward direction. On the contrary, the feed radiation is well-suppressed by the proposed transition, as shown in Fig. 9(b). It is seen that most of the power is bounded inside the transition attributed to the existence of the proper mode and is guided from the horn to the dielectric slab. From Fig. 9(b), it is also observed that the rapid decrease in feed radiation provides more space for the surface wave to expand, which benefits the formation of planar wavefront and high gain. For achieving higher gain, a straighter equiphase region for the surface wave at the slab is necessary [16]. However, the surface wave propagates along the dielectric slab and decays vertically to it [12]. To solve this issue, the leaky wave that is generated by the proposed transition is introduced to realize a transverse expansion of the surface wave into the free space. As shown in 9(b), the shape of the equiphase region for the radiating surface wave appears to be straighter than that of the antenna without the proposed transition in Fig. 9(a). It should be noted that part of the power along the transition is radiated away from the endfire direction in Fig. 9(b) at 22 GHz. The reason for this phenomenon can be explained by Fig. 8. As can be seen in Fig. 8, only the first two blocks of the transition operate in the proper mode, and the remaining blocks work in the leaky mode. Therefore, feed radiation is not perfectly suppressed by the first two blocks and can be radiated backward.

Fig. 10 shows the gain comparison between the proposed antenna with and without tapered transition. As shown, a maximum gain improvement around 9 dBi is achieved using tapered transition. For the antenna without tapered transition, the gain decreased sharply at some frequencies because of the interference between surface wave radiation and feed radiation. In short, with the aid of tapered multistrip transition, feed radiation is effectively suppressed, which helps realize the ideal excitation for an endfire antenna with maximum gain. Moreover, for achieving higher gain, a straighter equiphase region of the surface wave around the slab is obtained by the leaky wave that is generated by the proposed transition.

As analyzed in Sections II and III, the tapered multistrip transition helps improve the antenna bandwidth and transform the guided wave from the SIW to the surface wave around the dielectric slab with expanded wavefront. Without tapered multistrip transition, the IBW of the antenna is greatly deteriorated and antenna gain is not greatly improved. Therefore, the high-gain merit of the proposed antenna is accomplished by both the tapered multistrip transition and the loaded dielectric slab. However, even without dielectric slab loading, the antenna performance is still superior to other reported SIW horn antennas. Although guided waves, leaky waves, and surface waves

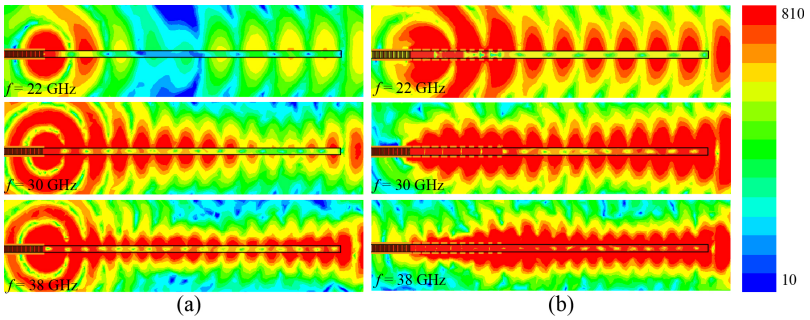

Fig. 9. *E*-field distributions of the dielectric-loaded SIW horn antenna at three different frequencies: (a) without the proposed transition and (b) with the proposed transition.

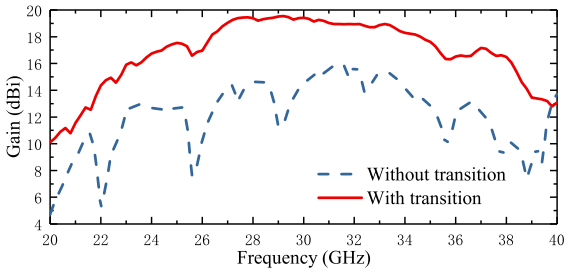

Fig. 10. Simulated gain of the proposed antenna with and without transition.

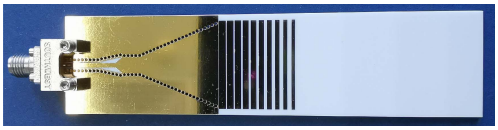

Fig. 11. Fabricated prototype.

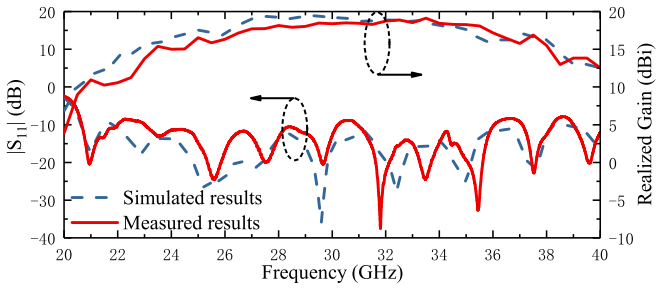

Fig. 12. Simulated and measured results of the proposed antenna.

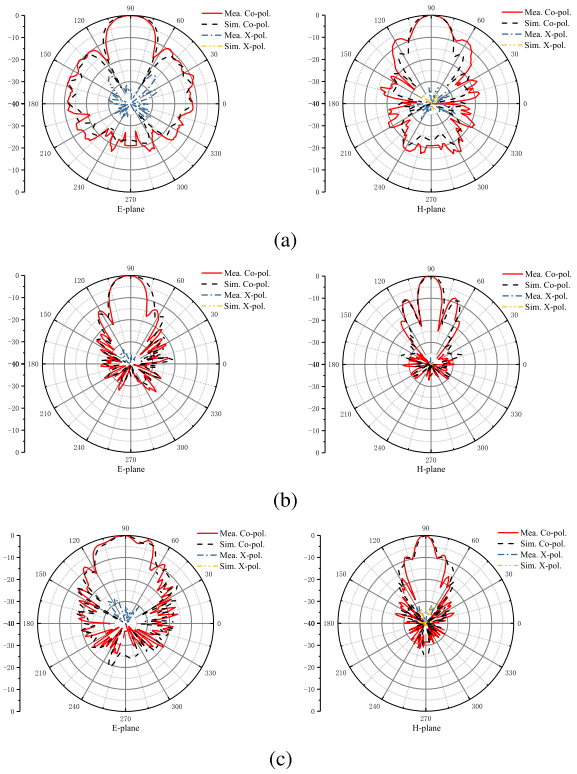

Fig. 13. Measured and simulated radiation patterns of the proposed SIW H-plane horn antenna. (a) 22 GHz. (b) 29 GHz. (c) 38 GHz.

all exist in the presented design, the proposed antenna is still named as an SIW horn antenna following the naming rules of other reported designs [4]–[6].

IV. Results and Discussions

Fig. 11 shows the fabricated prototype of the proposed antenna, which is printed on a Rogers RO4003 substrate with a thickness of 1.524 mm. The simulated and measured reflection coefficients of the proposed antenna are depicted in Fig. 12. The simulated IBW ranges from 20.64 to 38.38 GHz with $|S_{11}|$ smaller than -10 dB and the measured $|S_{11}|$ generally agree with the simulated results.

The simulated and measured gains are also plotted in Fig. 12. As shown, the measured gain is larger than 15 dBi within the frequency of 23.4–38 GHz, and the measured peak gain is 19.1 dBi at the frequency of 33.5 GHz. Fig. 13 shows the simulated and measured radiation patterns in both the E-plane and H-plane at three different frequencies. As can be seen, stable endfire radiation patterns are obtained across the whole bandwidth. It is worth pointing out that the simulated cross-pol radiation in the E-plane is rather small which cannot be shown in most of the figures. The measured cross polarization level is below -30 dB in both the main planes. A high FBR (>20 dB) is also obtained by the proposed antenna over the entire bandwidth and it can even reach 35 dB at the center frequency.

To demonstrate the merits of the proposed antenna, a comparison between the proposed antenna and other recently reported SIW horn and dielectric rod antennas is presented in Table I. As shown in Table I, the proposed antenna demonstrates much wider bandwidth and higher antenna gain than other reported SIW horn antennas. When compared with dielectric rod antennas, the proposed antenna also has much wider IBW and higher antenna gain, while keeping much lower profile of $0.1\lambda_0$.

TABLE I

COMPARISON BETWEEN THE PROPOSED ANTENNA AND OTHER REPORTED SIW HORN AND DIELECTRIC ROD ANTENNAS

Ref. No.	IBW (%)	Peak Gain (dBi)	Dimensions (λ_0^3)	Key Methods
[3]	16	8	$1.49 \times 1.20 \times 0.09$	Printed Uniform Transition
[4]	41	9.2	$2.35 \times 2.18 \times 0.26$	Perforated Dielectric Lens
[8]	6.5	10.3	$5.81 \times 3.02 \times 0.18$	Profiled Walls & Soft Surfaces
[17]	13.2	18	$7.07 \times \Phi 0.83$ (Circular)	Integrated Yagi-Uda and Dielectric Rod
[18]	20	17.8	$5.4 \times 0.18 \times 0.594$	Rectangular Dielectric Rod
This work	60	19.1	$6.98 \times 1.75 \times 0.10$	Printed Tapered Transition & Dielectric Loading

λ_0 is the free-space wavelength at the lowest operating frequency.

V. CONCLUSION

Using tapered multistrip transition and dielectric slab, a wideband high-gain SIW H-plane horn antenna has been presented. The tapered multistrip transition has been implemented for wideband operation based on the theory of coupled resonator. Besides, the optimal length of the dielectric slab is chosen as $6\lambda_0$ by the design principles of a dielectric rod with maximum gain. Moreover, the modal behaviors of the tapered multistrip transition have been investigated to reveal the gain enhancement mechanism. To validate the design concepts, a prototype has been designed, fabricated, and measured. The experimental results illustrate that the proposed antenna has a wide bandwidth of 60% and a high peak gain of 19.1 dBi. In addition, the proposed antenna exhibits endfire radiation patterns with low cross polarization and high FBR over the entire operating band. With these merits, the proposed antenna would be a very promising candidate for various mm-wave applications.

REFERENCES

[1] Y. Cassivi, L. Perregrini, P. Arcioni, M. Bressan, K. Wu, and G. Conciauro, "Dispersion characteristics of substrate integrated rectangular waveguide," *IEEE Microw. Wireless Compon. Lett.*, vol. 12, no. 9, pp. 333–335, Sep. 2002.

[2] M. Esquius-Morote, B. Fuchs, J. F. Zürcher, and J. R. Mosig, "A printed transition for matching improvement of SIW horn antennas," *IEEE Trans. Antennas Propag.*, vol. 61, no. 4, pp. 1923–1930, Apr. 2013.

[3] M. Esquius-Morote, B. Fuchs, J. Zurcher, and J. R. Mosig, "Novel thin and compact H-plane SIW horn antenna," *IEEE Trans. Antennas Propag.*, vol. 61, no. 6, pp. 2911–2920, Jun. 2013.

[4] Y. Cai, Y. Zhang, Z. Qian, W. Cao, and L. Wang, "Design of compact air-vias-perforated SIW horn antenna with partially detached broad walls," *IEEE Trans. Antennas Propag.*, vol. 64, no. 6, pp. 2100–2107, Jun. 2016.

[5] W. B. Park, J. M. Lee, S. Lee, Y. M. Park, and K. C. Hwang, "A 18–40 GHz substrate integrated waveguide H-plane horn antenna," *IEEE Trans. Antennas Propag.*, vol. 66, no. 11, pp. 6322–6327, Nov. 2018.

[6] H. Wang, D.-G. Fang, B. Zhang, and W.-Q. Che, "Dielectric loaded substrate integrated waveguide (SIW) H-plane horn antennas," *IEEE Trans. Antennas Propag.*, vol. 58, no. 3, pp. 640–647, Mar. 2010.

[7] L. Wang, X. Yin, S. Li, H. Zhao, L. Liu, and M. Zhang, "Phase corrected substrate integrated waveguide H-plane horn antenna with embedded metal-via arrays," *IEEE Trans. Antennas Propag.*, vol. 62, no. 4, pp. 1854–1861, Apr. 2014.

[8] N. Bayat-Makou and A. A. Kishk, "Substrate integrated horn antenna with uniform aperture distribution," *IEEE Trans. Antennas Propag.*, vol. 65, no. 2, pp. 514–520, Feb. 2017.

[9] C. A. Balanis, *Antenna Theory: Analysis Design*. Hoboken, NJ, USA: Wiley, 2005.

[10] L. Wang, M. Garcia-Vigueras, M. Alvarez-Folgueiras, and J. R. Mosig, "Wideband H-plane dielectric horn antenna," *IET Microw., Antennas Propag.*, vol. 11, no. 12, pp. 1695–1701, 2017.

[11] T. Ando, J. Yamauchi, and H. Nakano, "Rectangular dielectric-rod fed by metallic waveguide," *IEE Proc.-Microw., Antennas Propag.*, vol. 149, no. 2, pp. 92–97, Apr. 2002.

[12] J. L. Volakis, *Antenna Engineering Handbook*. New York, NY, USA: McGraw-Hill, 2007.

[13] H. Ehrenspeck and H. Poehler, "A new method for obtaining maximum gain from Yagi antennas," *IRE Trans. Antennas Propag.*, vol. 7, no. 4, pp. 379–386, Oct. 1959.

[14] A. Mehdipour and G. V. Eleftheriades, "Leaky-wave antennas using negative-refractive-index transmission-line metamaterial supercells," *IEEE Trans. Antennas Propag.*, vol. 62, no. 8, pp. 3929–3942, Aug. 2014.

[15] S. M. Hanham, T. S. Bird, A. D. Hellicar, and R. A. Minasian, "Evolved-profile dielectric rod antennas," *IEEE Trans. Antennas Propag.*, vol. 59, no. 4, pp. 1113–1122, Apr. 2011.

[16] T. Ando, I. Ohba, S. Numata, J. Yamauchi, and H. Nakano, "Linearly and curvilinearly tapered cylindrical-dielectric-rod antennas," *IEEE Trans. Antennas Propag.*, vol. 53, no. 9, pp. 2827–2833, Sep. 2005.

[17] M. Nasir, Y. Xia, M. Jiang, and Q. Zhu, "A novel integrated Yagi–Uda and dielectric rod antenna with low sidelobe level," *IEEE Trans. Antennas Propag.*, vol. 67, no. 4, pp. 2751–2756, Apr. 2019.

[18] Y. Hou, Y. Li, Z. Zhang, and Q. Xue, "Rectangular dielectric rod antenna fed by air-substrate parallel strip line," *IEEE Trans. Antennas Propag.*, vol. 67, no. 10, pp. 6308–6316, Oct. 2019.